# Electronic Factors Controlling Bandwidths in Oxides with the Perovskite and Cadmium Halide Structures

**Jeremy K. Burdett* and Stephen A. Gramsch**

Department of Chemistry, James Franck Institute, and Science and Technology Center for Superconductivity, The University of Chicago, 5735 South Ellis Avenue, Chicago, Illinois 60637

*Received March 9, 1994*[⊗]

The electronic structure of oxides with the perovskite and cadmium halide structures are derived using tight-binding theory and the angular overlap model. The control of the form of the energy bands by the presence of vertex- (perovskite) and edge-sharing (cadmium halide) of the coordination octahedra is first explored using one-dimensional examples. For one-, two-, and three-dimensional structures of the perovskite type, a very interesting result is uncovered. It is shown that on the band model a band gap may only arise if the oxygen 2s orbital is included in the orbital problem. Prediction of the magnitude of the band gaps in $d^6$ perovskites is thus not a simple matter. This band structure, derived from tight-binding theory via the construction of Bloch orbitals, is compared with an energy band scheme based on local crystal field orbitals and covalent metal–oxygen interactions, which has traditionally been used in this area.

## Introduction

A problem of long-standing interest in solid state inorganic chemistry is the correlation of structural features characteristic of a particular compound or class of materials with its physical properties, often electronic and magnetic behavior. This is an area which has received a recent stimulus with the discovery of high-temperature superconductivity in complex copper oxides. One effective route to understanding the intricate interplay of crystal and electronic structure and physical properties is consideration of orbital interactions in the solid state.[1] Although such one-electron models neglect the important effects of electron correlation, and so must be used with caution in strongly correlated systems, they are unrivaled at providing insights into the properties of complex materials.[2] Especially important is the tracing of features of the electronic densities of states to fundamental interactions between the structural building blocks of the solid. Recently, building on earlier concepts, Kemp and Cox suggested[3] that the difference in properties of the two materials $LaCoO_3$ (semiconducting to metallic transition)[4] and $LiCoO_2$ (insulating), both of which formally contain $d^6$ Co(III), is directly a result of the different d-block bandwidths in the two materials, and hence different band gaps. $LaCoO_3$ has the perovskite structure and $LiCoO_2$ a rock salt derivative or filled-up $CdCl_2$ structure. Since the metal atoms are octahedrally coordinated in both compounds, the wider band in the perovskite case was argued as arising from the strong $\sigma$ interactions of the perovskite **1** compared to the poorer $\sigma + \pi$ interactions in the cadmium halide arrangement, as shown in **2**. An identical structural relationship exists between $d^7$ Ni(III) compounds. $LaNiO_3$ is metallic at all temperatures,[5] but $LiNiO_2$ is ferromagnetic and insulating.[6] (Recent experimental evidence suggests that $LiNiO_2$ also orders antiferromagnetically below 10 K.[7]) Here the different electrical properties of these two systems are also viewed in terms of their differing bandwidths; in the present work, we also show how this structural–electronic problem is really a rather broad one and how a study of the band structure of oxides of this type using simple tight-binding ideas and the angular overlap model[8] shows some rather striking structure–property consequences of the geometrical structure.


**1**

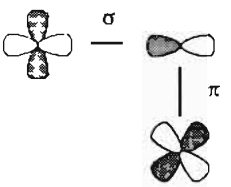


**2**

## The Electronic Problem

$LaCoO_3$ and $LaRhO_3$, both with the $d^6$ configuration about the metal center, adopt the perovskite structure (Figure 1a)[9] although whereas the Co compound is essentially an ideal perovskite with a very slight rhombohedral distortion, the Rh analog has a distorted structure of the familiar $GdFeO_3$ type.[10] The band gap is 1.6 eV in the latter, which is an insulator, but 0.1 eV in the former,[11] and it is this small gap which leads to some interesting effects at higher temperatures as a result of

⊗ Abstract published in *Advance ACS Abstracts,* August 15, 1994.

(1) Goodenough, J. B. *Prog. Solid State Chem.* **1971**, *5*, 145.
(2) (a) Hoffmann, R. *Solids and Surfaces: A Chemist's View of Bonding in the Solid State*; VCH Publishers: New York, 1988. (b) Burdett, J. K. *Chemical Bonding in Solids*; Oxford University Press: New York, 1995.
(3) Kemp, J. P.; Cox, P. A. *J. Phys.: Condens. Matter* **1990**, *2*, 9653.
(4) Raccah, P. M.; Goodenough, J. B. *Phys. Rev.* **1967**, *155*, 932.
(5) (a) Goodenough, J. B.; Raccah, P. M. *J. Appl. Phys.* **1965**, *36*, 1031. (b) Koehler, W. C.; Wollan, E. O. *J. Phys. Chem. Solids* **1957**, *2*, 100.
(6) Kemp, J. P.; Cox, P. A.; Hodby, J. W. *J. Phys.: Condens. Matter* **1990**, *2*, 6699.
(7) Riemers, J. N.; Dahn, J. R.; Greedan, J. E.; Stager, C. V.; Liu, G.; Davidson, I.; von Sacken, U. *J. Solid State Chem.* **1993**, *102*, 542.
(8) Burdett, J. K. *Molecular Shapes*; Wiley-Interscience: New York, 1980; p 7 ff.
(9) Wold, A.; Post, B.; Banks, E. *J. Am. Chem. Soc.* **1957**, *79*, 6365.
(10) Müller, O.; Roy, R. *The Major Ternary Structural Families*; Springer-Verlag: New York, 1975; p 187.
(11) Cox, P. A. *Transition Metal Oxides*; Clarendon Press: Oxford, U.K., 1992; p 115.

0020-1669/94/1333-4309$04.50/0 

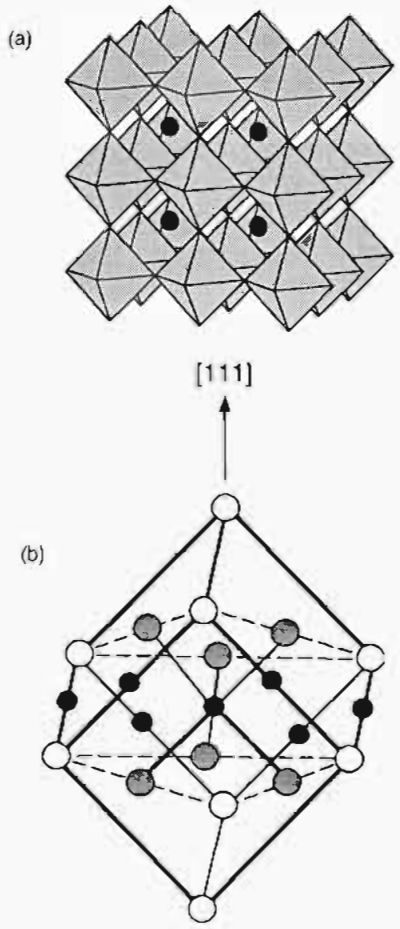


**Figure 1.** (a) Polyhedral representation of the perovskite structure. (b) Rhombohedral unit cell for $LiNiO_2$: small filled circles, Ni; unfilled circles, O. Li atoms which occupy the planes between O layers have been omitted for clarity.

thermal excitation of the charge carriers across it.[4] What are the factors which control its size? Are the usual considerations developed by the molecular chemist concerning octahedral $e_g/t_{2g}$ splittings applicable to this problem or are the important parameters different? Octahedrally coordinated metals with similar local but different extended structures often behave differently. As mentioned above, although the nickel atom is nominally trivalent in both cases ($d^7$), the perovskite $LaNiO_3$, exhibits metallic conductivity down to 4 K, while $LiNiO_2$ is an insulator. This suggests that the bandwidth in $LaNiO_3$ is sufficiently wide to support metallic conduction via a partially filled band. The presumably localized electronic description found for $LiNiO_2$ suggests a narrower band. A close examination of the electronic structures of these Ni systems allows some general conclusions which help address important structural issues governing the formation of energy bands and associated band gaps in transition metal oxides.

Although $LaNiO_3$, like $LaCoO_3$, is a rhombohedrally distorted perovskite in which the deviation from ideality is the result of small displacements of the oxygen atoms from their ideal positions along the Ni—O bond directions, the compound may, to a very good approximation, be considered an undistorted, ideal perovskite. A slice through the equatorial plane of the Ni atoms in a given layer of the perovskite reveals a corner-shared square net of stoichiometry $NiO_2$, as shown in **3**, a structural motif identical to that also encountered in all cuprate superconductors. We shall ignore the presence of the large A cation in our calculations (except for the electrons it contributes), and so the structure which we call "perovskite" is really that of $ReO_3$. The structure of $LiNiO_2$[12] may be regarded as a derivative of the rock salt arrangement of NiO, with alternate

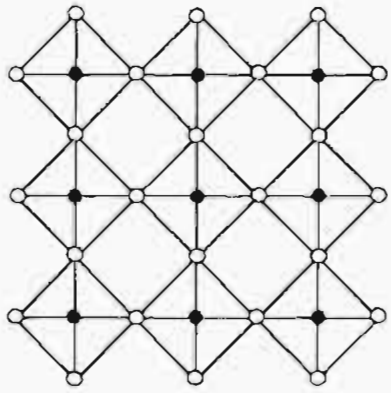

**3**

planes of Ni atoms along [111] replaced by Li atoms (Figure 1b). The layer of stoichiometry $NiO_2$ which lies between the planes of Li atoms has effectively the cadmium chloride structure, a two-dimensional network of edge-sharing octahedra, in which each $NiO_6$ octahedron shares all 12 of its edges (**4**).

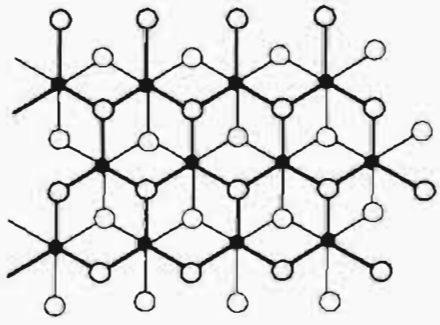

**4**

Thus, whereas the perovskite framework of $LaNiO_3$ is characterized in two dimensions by a square $NiO_2$ net, the $NiO_2$ layer in $LiNiO_2$ has hexagonal symmetry. We shall consider the electronic properties of this layer in this paper. Differing steric requirements of $LiO_6$ and $NiO_6$ octahedra at their equilibrium metal—oxygen distances enforce elongation of the ideal cube of rock salt NiO along the body diagonal [111] to give the rhombohedral structure of $LiNiO_2$, as shown in Figure 1b. This particular structural feature gives $LiNiO_2$ its inherently two-dimensional nature and separates the $NiO_2^-$ layers from the intervening close-packed planes of Li atoms. In both $LaNiO_3$ and $LiNiO_2$, the Ni—O bond length is 1.94 Å, although the $NiO_6$ octahedra are slightly more distorted in $LiNiO_2$ than in $LaNiO_3$. Importantly, however, the crystal structures of both $LaNiO_3$ and $LiNiO_2$ may be viewed in terms of linked arrays of $NiO_6$ octahedra.

One approach to the band structures of such octahedrally coordinated transition metal oxides (a "phenomenological" approach[1]) is shown in Figure 2. Mixing of Ni d states with oxygen valence orbitals ("the ligand field") splits the d levels into $t_{2g}$ and $e_g$ sets to give the classical local scheme pictured in Figure 2a, the magnitude of the interaction dependent upon the relevant Ni d/O overlaps. The $t_{2g}$ set ($\pi$ symmetry with respect to the ligand p set) is therefore less destabilized than the $e_g$ set ($\sigma$ to the ligand p orbitals). The size of the $t_{2g}$—$e_g$ gap ($\Delta$) is set by the difference in magnitude of the two types of interactions.[1,11,13] These $t_{2g}$ and $e_g$ levels then broaden into

(12) Wyckoff, R. W. G. *Crystal Structures*, 2nd ed.; Wiley-Interscience: New York, 1964; Vol. 2, p 292.
(13) Cox, P. A. *The Electronic Structure and Chemistry of Solids*; Oxford University Press: New York, 1987; p 72.

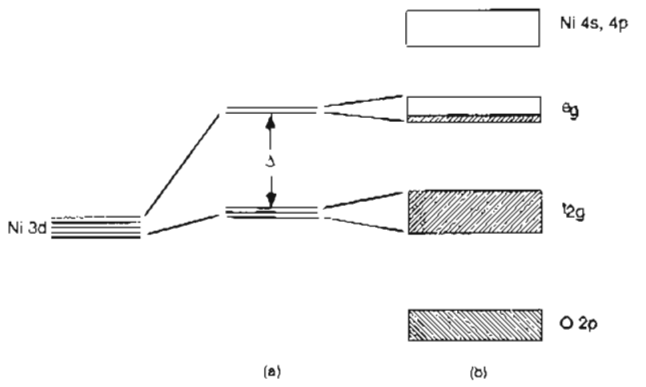


**Figure 2.** "Phenomenological" electronic band structure in transition metal oxides: (a) local model incorporating differential destabilization of Ni 3d orbitals to $t_{2g}$ and $e_g$ sets as a result of octahedral coordination by oxygen; (b) energy bands formed by interaction of the $NiO_6$ octahedron with neighboring octahedra in the extended solid.

bands by interaction with their environment as in Figure 2b. Using this "phenomenological" model, both $LaNiO_3$ and $LiNiO_2$ are predicted to be metallic, since the band structure dictates a quarter-filled $e_g$ band for each. If the band is sufficiently wide, a localization (analogous to the Hubbard[14] type for the antiferromagnetic insulating state) or generation of a high-spin ferromagnetic insulating state will be less stable than that of the metallic state described by a delocalized wavefunction. As noted earlier, it has been argued that the width of the band is determined by the magnitude of the interactions between adjacent $\sigma$-type bond orbitals as shown in **1** and **2**. A wider band compared to that for the cadmium halide structure has been predicted for the perovskite. Metallic behavior is expected for the system with the wider band, a result consistent with experiment. However, the phenomenological band structure may hide important electronic features which become clear when energy bands are constructed from Bloch functions in the traditional way. It will turn out that there is only a hint of the relevance of **1** and **2** in the real band structure.

## One-Dimensional-Chain Models

The best way to understand the dependence of bandwidth or relative band location on structure is to obtain a detailed understanding of the origin of the dispersion in the bands themselves.[2] A good place to start is a system of reduced dimensionality. A closer look at the structures of the nickel–oxygen frameworks in $LaNiO_3$ and $LiNiO_2$ shows that these units are essentially built up from three interpenetrating one-dimensional chains of octahedra, each containing an octahedrally coordinated metal atom. In the case of perovskite, the chains are corner-shared (**5**), while in the cadmium halide arrangement, the chains are edge-shared (**6**). The local-orbital structure for the octahedron using the angular overlap model (AOM) is shown in **7**. This is a simple parameterization[8,15] of the orbital problem where the starting energies of the interacting orbitals are different. The AOM scheme leads to the parameters $e_\sigma$ and $e_\pi$, which measure the strength of $\sigma$ and $\pi$ interactions *via* second-order perturbation theory. This local picture (**7**) will provide useful insights into the structures of extended systems, as it is this unit which is the basis for the two types of one-dimensional chains which constitute the Ni–O frameworks of the two structures of interest. For the $NiO_6$ octahedron, the $t_{2g}$ and $e_g$ orbitals are separated by $3e_\sigma - 4e_\pi$. Also shown in **7** are energies from an extended Hückel (EH) calculation on this unit

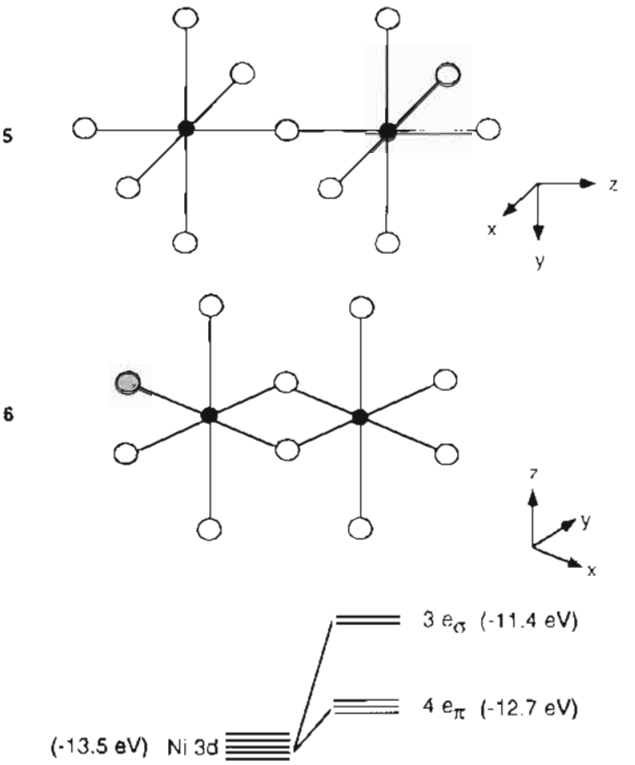


**7**

with a Ni–O distance of 1.94 Å and p orbitals only on oxygen, which will serve as a reference for AOM energy values derived for band orbitals. (The parameters used are listed in the Appendix.) From this picture, $e_\pi = 0.2$ eV and $e_\sigma = 0.7$ eV.

The band structures of the chains of **5** and **6** are derived in several places (see for examples refs 16 and 17). Particularly interesting here though will be the role of the s and p orbitals on the bridging oxygen atom. Initially, we use only p orbitals on all oxygen atoms and d orbitals on nickel. The orbital topologies appropriate for the interaction of metal $t_{2g}$ and $e_g$ type orbitals (these are not the correct symmetries in these infinite chains, but we will use such labels as a convenience) with ligand p orbitals are simply generated by symmetry and are shown in Figure 3 for the one-dimensional chain removed from the three-dimensional perovskite. For the degenerate pair of $t_{2g}$ orbitals in Figure 3a,b, no p$\pi$ orbital contribution exists at the point $\Gamma$, the zone center, so the level is exactly M–O nonbonding at this point. At the zone edge, point X, the metal crystal orbital has the proper symmetry to interact in a $\pi$-antibonding fashion with the p orbitals on the intervening oxygen atoms. This leads to a destabilization at X and gives the $t_{2g}$ band its dispersion. The nondegenerate crystal orbital pictured in Figure 3c remains nonbonding throughout the one-dimensional zone. An AOM treatment of the dispersive bands proceeds in the usual way[15] from the solution of the secular determinant of eq 1, appropriate to the doubly degenerate set

$$\begin{vmatrix} H_{dd} - E & H_{dp}(\mathbf{k}) - ES_{dp}(\mathbf{k}) \\ H_{pd}(\mathbf{k}) - ES_{pd}(\mathbf{k}) & H_{pp} - E \end{vmatrix} = 0 \qquad (1)$$

of interactions shown in **8**, for a unit cell of the vertex-sharing chain. Using the Hückel $\alpha$ and $\beta$ labels for notational convenience, as in eq 2, the roots are $E \approx \alpha_p + 4\beta^2 \sin^2(ka/2)/|(\alpha_p - \alpha_d)|$ and $E \approx \alpha'_d - 4\beta^2 \sin^2(ka/2)/|(\alpha_p - \alpha_d)|$ or, introducing the parameter of the angular overlap model,[8] $E$

(14) Hubbard, J. *Proc. R. Soc. London*, **1963**, *A276*, 38; **1964**; *A277*, 237; **1964**, *A281*, 401.

(15) Burdett, J. K. *Adv. Inorg. Chem. Radiochem.* **1978**, *21*, 113. Atanasov, M. A.; Schmidtke, H.-H. *Chem. Phys.* **1988**, *124*, 205.

(16) Burdett, J. K. *Prog. Solid State Chem.* **1984**, *15*, 173.

(17) Whangbo, M.-H.; Foshee, M. J. *Inorg. Chem.* **1981**, *20*, 113.

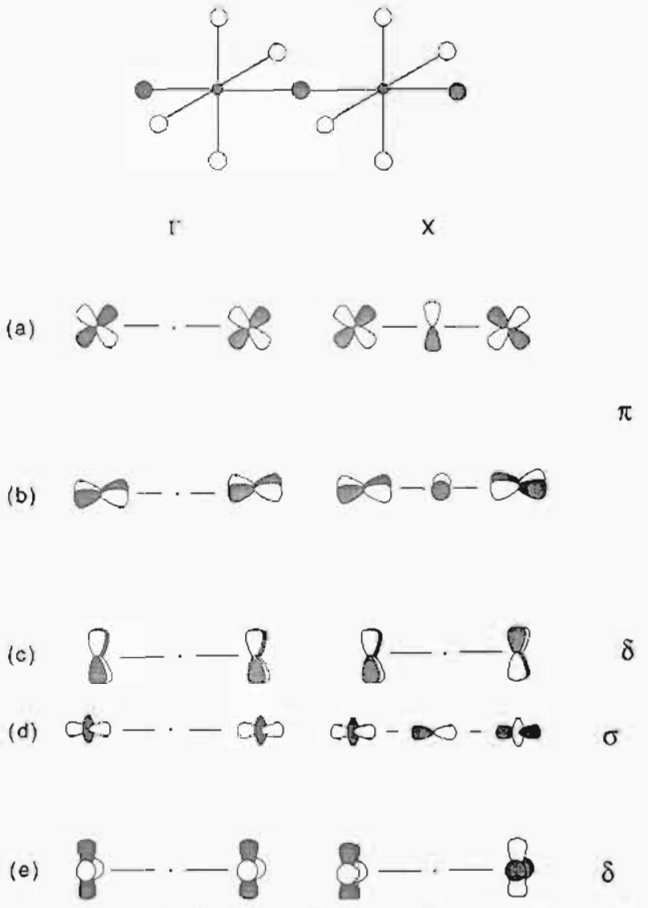


**Figure 3.** Crystal orbitals formed by interaction of 3d orbitals on Ni with O 2p valence orbitals for the one-dimensional vertex-sharing chain of octahedra appropriate for the perovskite structure.

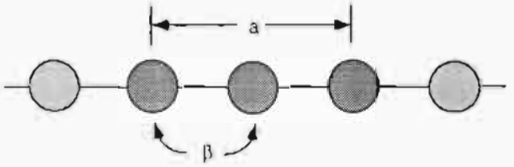


8

$$\begin{vmatrix} \alpha'_d - E & 2\beta \sin(ka/2) \\ 2\beta \sin(ka/2) & \alpha_p - E \end{vmatrix} = 0 \qquad (2)$$

$\approx \alpha_p - 4e_\pi \sin^2(ka/2)$ and $E \approx \alpha'_d + 4e_\pi \sin^2(ka/2)$, where $e_\pi = -\beta/|(\alpha_p - \alpha_d)|$. Here $\alpha'_d$ is the $\alpha$ value of the appropriate orbital taking into the account the interactions of the other ligands perpendicular to the chain and $\alpha_d$ is the energy of the unperturbed d levels. We are only interested here in the higher energy root, the "metal d orbital", which leads to an energy of $\alpha'_d$ at Γ and $\alpha'_d + 4e_\pi$ at X. The bandwidth of the Figure 3a,b pair of bands is thus equal to $4e_\pi$. For this degenerate pair of $\pi$ bands, $\alpha'_d = \alpha_d + 2e_\pi$, while for the nondegenerate and nondispersive $\delta$ band, $\alpha'_d = \alpha_d + 4e_\pi$.

Similar considerations lead to the dispersion behavior for the two bands belonging to the $e_g$ set of the perovskite-like chain. For the $d_{z^2}$ basis function (Figure 3d) $\alpha'_d = \alpha_d + e_\sigma$, and solution of the secular determinant for this case leads to energies of $e_\sigma$ at Γ and $5e_\sigma$ at X. The dispersion of the band along the chain is thus $4e_\sigma$. There is no dispersion associated with the $d_{x^2-y^2}$ orbital (Figure 3e), since it is of $\delta$ symmetry with respect to the oxygen atoms and thus finds no symmetry match with a bridge orbital. It remains equienergetic, $E = \alpha_d + 3e_\sigma$, at all points in the one-dimensional zone. It is helpful to note that the solution of the secular determinant for these various band orbitals results in the centering of the set of energy bands about

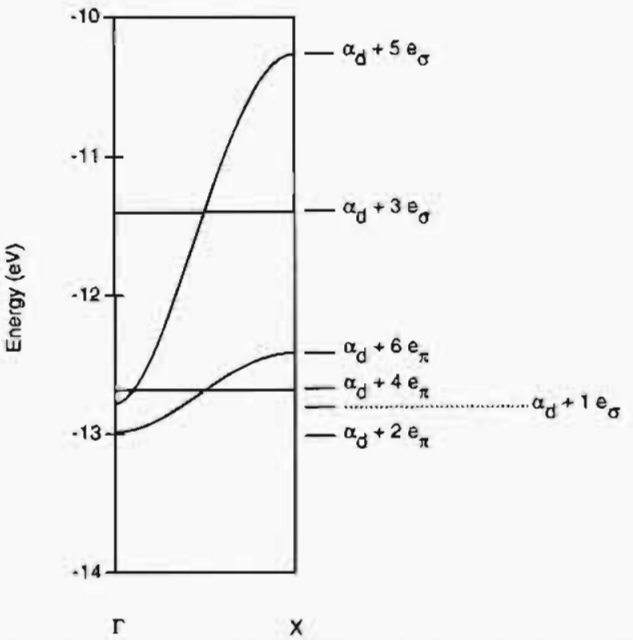


**Figure 4.** Calculated energy bands for Ni d-orbital-based crystal orbitals in the one-dimensional vertex-sharing chain of octahedra. The values at the right of the panel are those predicted using the AOM and the numerical results from 7.

**Table 1.** Crystal Orbital Energies[a] (eV) for Ni d-Block Bands of the Vertex-Sharing One-Dimensional Chain

| Ni orbital | AOM energy, Γ | Γ, predicted | Γ, calcd | AOM energy, X | X, predicted | X, calcd |
|---|---|---|---|---|---|---|
| $d_{xz}$ | $2e_\pi$ | −13.1 | −13.0 | $6e_\pi$ | −12.3 | −12.4 |
| $d_{yz}$ | $2e_\pi$ | −13.1 | −13.0 | $6e_\pi$ | −12.3 | −12.4 |
| $d_{xy}$ | $4e_\pi$ | −12.7 | −12.7 | $4e_\pi$ | −12.7 | −12.7 |
| $d_{x^2-y^2}$ | $3e_\sigma$ | −11.4 | −11.4 | $3e_\sigma$ | −11.4 | −11.4 |
| $d_{z^2}$ | $e_\sigma$ | −12.7 | −12.8 | $5e_\sigma$ | −10.5 | −10.3 |

[a] Calculated energies include the effects of metal−metal bonding along the chain.

the levels $4e_\pi$ for the $t_{2g}$ bands and $3e_\sigma$ for the $e_g$ bands. The band dispersion shown in Figure 4 from an extended Hückel tight-binding (EHTB) calculation gives a bandwidth and crystal orbital energies quite close those predicted from the numerical values derived from 7 as shown at the right of the panel.

The bandwidths calculated by the AOM formalism are in fact slightly larger than those produced by the actual calculation which appear in Table 1. This is due to direct interactions between the metal centers in the chain. The effect will depend upon the metal−metal distance and, anticipating our results for the edge-sharing chain, will become larger as the metal−metal distance decreases, and is therefore more pronounced for that case than for this one. In Figure 3a, the doubly degenerate $t_{2g}$-type wavefunction is metal−oxygen nonbonding at the point Γ, but also metal−metal antibonding, an effect which results in the small destabilization of the crystal orbital at this point, in addition to what is predicted on the basis of the AOM treatment. Likewise, the same crystal orbital is metal−metal bonding at the zone edge X, and thus the energy of the band is stabilized with respect to the value calculated with the AOM. The opposite effects are operative in the $e_g$ band whose orbital interactions are described in Figure 3d. This band is metal−metal bonding at the point Γ, and thus the energy level will be stabilized relative to the value predicted using the metal−oxygen interactions only. At the point X, in contrast, the level will be destabilized due to metal−metal antibonding, resulting in a bandwidth greater than the value predicted using the AOM. When the calculations are repeated with the Ni−Ni overlap integrals set equal to zero, the crystal orbital energies predicted

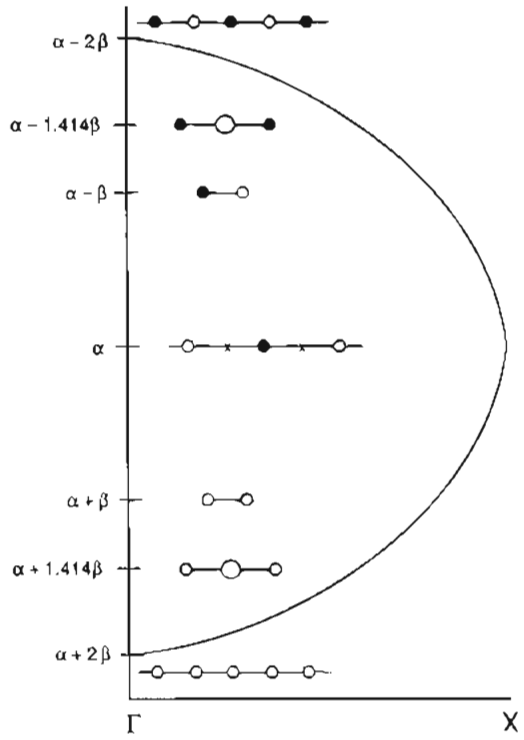


**Figure 5.** Dispersion picture for a homoatomic chain of atoms, showing also the energies of diatomic and triatomic units.

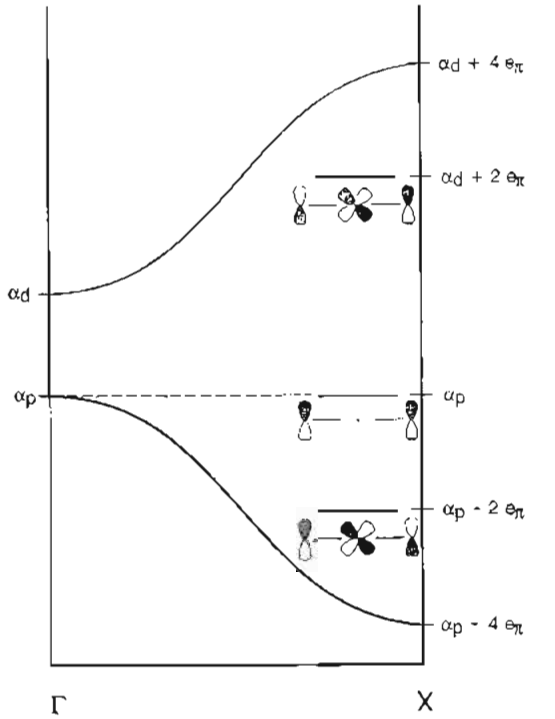


**Figure 6.** Dispersion picture for a heteroatomic chain of atoms, showing also the energies of a triatomic unit.

from the AOM are in fact nearly identical to those calculated using the figures from 7, as shown in Table 1.

An important result from this discussion is that these dispersion pictures do not coincide with the "phenomenological" picture of Figure 2. Our results arises through our insistence on treating on an equal footing the local interactions of an oxygen p orbital with the metal orbitals, along with the extended coupling of the metal center through the bridging orbital. In the model of Figure 2, one is significantly larger than the other. Another result is immediately apparent too. Notice that the tops of the bands are destabilized more than a $t_{2g}$ d$\pi$ or $e_g$ d$\sigma$ orbital in the hypothetical isolated $NiO_6$ molecule ($4e_\pi$ or $3e_\sigma$). This comes rather simply from the details of eq 1. The *mean* value of the orbital energy across the zone is, however, $4e_\pi$ or $3e_\sigma$. It is interesting to compare the energies of this heteroatomic ...ABAB... chain with those of a simple Hückel treatment of the homoatomic one. In some respects, the AOM model plays an analytic role in such heteroatomic systems analogous to the one that the Hückel model plays in homoatomic ones. Figure 5 shows the energy bands of a two-atom ...BBBB... cell **8** where the orbitals are linked to their neighbors by an interaction integral $\beta$. The interactions of this generic picture of course can be of $\lambda = \sigma, \pi$, or $\delta$ type. The dispersion of the bands is given by $E = \alpha \pm 2\beta \cos(ka/2)$ where $a$ is the repeat parameter. The width of the band is $4\beta$. Also shown are the energy levels of the "diatomic molecule", $E = \alpha \pm \beta$, and those of the "triatomic molecule" BBB, $E = \alpha, \alpha \pm 1.414\beta$. It is clearly seen that the top of the band lies above the upper molecular levels and the bottom of the band below the lower molecular levels. For the heteroatomic chain, the dispersion of the two bands from eq 1 is shown in a similar way in Figure 6. (The width of each is $4e_\lambda$.) The energy levels of an isolated BAB "molecule" (**9**) within the heteroatomic chain are also shown. Again they lie within the band width of the two bands. The point to be made here is that, just as one would not use the levels of the BBB triatomic to derive the levels of the bands of the infinite homoatomic chain, we should not follow this route for the heteroatomic one.

Generating the energy bands of the one-dimensional chain **6** from the hexagonal layer structure is a little more complex because, unlike the case of the vertex-sharing chain, the bridge orbitals of the edge-sharing chain can mix in both $\sigma$ and $\pi$ fashion with those of the metal. However, if the M—O—M angles are 90°, then the bridge p orbitals which are purely $\sigma$ for one metal are purely $\pi$ for the other. The five distinct crystal orbital types which make up the d-block bands of the chain are given at Γ and X in Figure 7. The orbitals are labeled according to their parity (symmetric or antisymmetric) with respect to (first) the mirror plane containing the $MO_2M$ unit and (second) the plane perpendicular to it. Both planes are good symmetry elements throughout the whole one-dimensional zone. The calculated behavior of the a, b pair of "$t_{2g}$" bands shown in Figure 8a using only metal—oxygen $\pi$ interactions in the band calculation is similar to that of the dispersive $\pi$ bands of the perovskite chain; one is M—O nonbonding at the Γ point and antibonding at the X point, and the other the converse. The predictions of the AOM are shown for comparison. (We point out that the coordinate system we have chosen in **6** dictates a mixing of the $d_{xz}$ and $d_{yz}$ orbitals in this frame to form linear combinations with the character we have illustrated in Figure 7a,b.) With two $\pi$ orbitals in the bridge which can interact with the metal d orbital, a larger destabilization at X for this chain than in the perovskite case might have been expected, but this is exactly canceled by the normalization factor ($1/2^{1/2}$) for the pair of bridging orbitals. The dispersion of these bands is thus identical ($4e_\pi$) to that for the perovskite chain. The third $\pi$ band has no dispersion; a linear combination of bridging oxygen p orbitals may be written which smoothly goes from one to the other between Γ and X. The behavior of the $e_g$ bands (Figure 3d,e) using $\sigma$ interactions only is dispersion-free, for the same reasons; they both have an energy of $3e_\sigma$ at both the

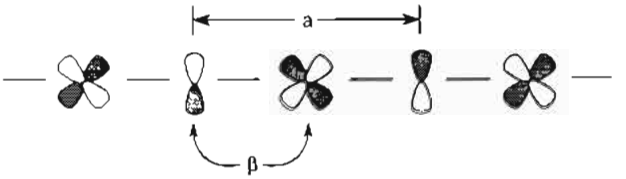


**9**

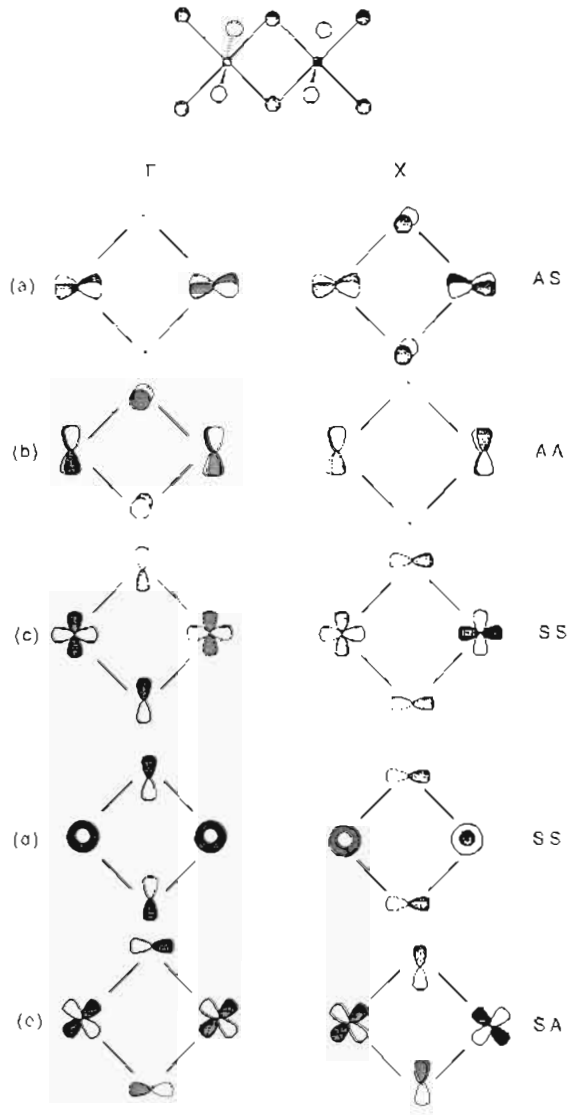


**Figure 7.** Crystal orbitals formed by interaction of 3d orbitals on Ni with O 2p valence orbitals for the one-dimensional edge-sharing chain of octahedra appropriate for the two-dimensional hexagonal net of the cadmium halide-like $NiO_2$ substructure. Labels follow the discussion in the text.

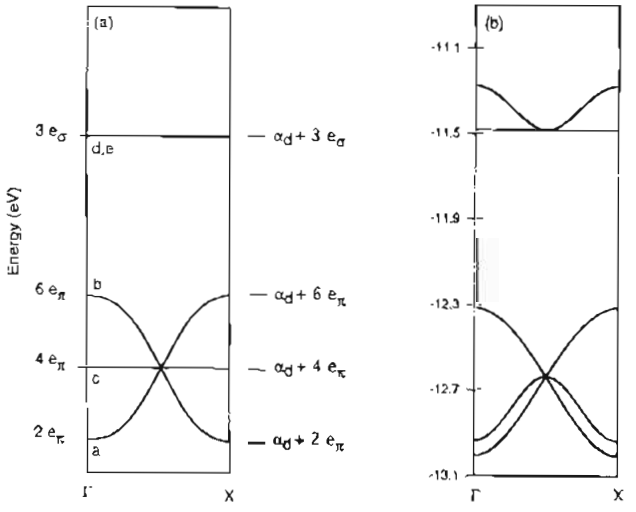


**Figure 8.** Energy bands for Ni d-orbital-based crystal orbitals for the edge-sharing chain of octahedra, based on the assumptions of the angular overlap model, considering only nickel–oxygen interactions: (a) without $e_g/t_{2g}$ mixing; (b) with $e_g/t_{2g}$ mixing.

X and Γ points. Notice however that one band from the $\sigma$ manifold and one from the $\pi$ manifold (Figure 3c,d) are of the same symmetry and thus may mix together. This is an important result and one which we have used before[18] to explore the "failure" of simple Jahn–Teller arguments in predicting local geometric features in transition metal dioxide structures of the rutile type. The new calculated band structure which includes such mixing is shown in Figure 8b.

The pictures developed in Figures 7 and 8 for the edge-sharing chain have completely ignored the effects of metal–metal bonding across the shared edge of the octahedron. In the perovskite chain these were of little importance, but here the Ni–Ni distance is only 2.74 Å, compared to 2.49 Å in the fcc metal.[19] Since the $e_g$ bands contain strong metal–oxygen $\sigma$ interactions, the effect of metal–metal interactions is expected to be smaller here than in the $t_{2g}$ bands, where the metal character is larger. Indeed, a useful picture of the $t_{2g}$ levels in $MO_2$ nets with the cadmium halide structure may be generated[20] by study of these interactions alone. Such would be the case if metal–metal bonding is on the same order of, or even greater than, the interactions between metal and oxygen. We therefore expect a much larger influence of metal–metal interactions in the cadmium halide-like structure than in the perovskite. A calculated dispersion diagram for a hypothetical metal-only chain with M–M distance equal to those used in the edge-sharing oxygen-containing chain is shown in Figure 9a. The overall width is about 1.5 eV, and when compared with the oxygen-only $\pi$ splittings from the AOM, these metal–metal interactions are clearly rather important. They show up in a striking fashion when comparisons are made between the complete band structure (Figure 9b) and that using the metal–oxygen interactions only (Figure 8b). For example, the dispersion-free crystal orbital (Figure 7c) is actually metal–metal $\sigma$ bonding at Γ and metal–metal $\sigma$ antibonding at X, leading to a highly dispersive band in the calculation of Figure 9b. For the M–M $\pi$-type band, orbital a of Figure 7, the orbital energy is raised at Γ due to antibonding interactions across the bridge but stabilized at X. Finally, the $\delta$-type band energy is stabilized at Γ but raised at X. Similar arguments lead to the changes in the dispersion of the $e_g$ bands. Recall that, in the vertex-sharing chain, the $e_g$ bandwidth was enhanced by these metal–metal interactions as it appears to be here too but in a more dramatic fashion. These arguments are standard ones which have been used before[16] but are worth repeating because they have an interesting bearing on the overall picture as we will see. Table 2 gives the observed crystal orbital energies from an actual band calculation on the edge-sharing chain compared with those predicted at various stages in the above discussion.

The $t_{2g}$ bandwidth in the edge-sharing chain is predicted and found to be nearly double that in the vertex-sharing chain (0.6 eV compared to 1.1 eV), but the $e_g$ band is predicted to be much wider in the vertex-sharing chain as compared to its edge-sharing relative, and this result leads to the absence of a gap between $e_g$ and $t_{2g}$ or $\sigma$ and $\pi$ bands. In the perovskite chain, at one point in the zone (Γ), $d_{z^2}$ is identically nonbonding, and at another, it is maximally antibonding. In the edge-sharing chain, however, both $d_{z^2}$ and $d_{x^2-y^2}$ orbitals overlap with orbitals on the bridging oxygen atoms at all points in the zone, and thus the symmetry constraints of this 90° chain dictate that these orbitals destabilize the $e_g$ crystal orbitals at all points, leading to a much narrower band than in the perovskite case. Importantly, the width of the bands in the edge-sharing case is dominated by metal–metal interactions but the width of the vertex-sharing case by metal–oxygen interactions. In a qualitative sense, the phenomenological model of Figure 2 is appropri-

(18) Burdett, J. K.; Miller, G. J.; Richardson, J. W.; Smith, J. V. *J. Am. Chem. Soc.*, **1988**, *110*, 8064.
(19) Reference 12, Vol. 1, p 10.
(20) Burdett, J. K.; Hughbanks, T. *Inorg. Chem.* **1985**, *24*, 1741.

**Table 2.** Crystal Orbital Energies (eV) for Ni d-Block Bands of the Edge-Sharing One-Dimensional Chain

| | metal−metal bonding not included | | | | | | metal−metal bonding included | |
|---|---|---|---|---|---|---|---|---|
| Ni orbital | AOM energy, Γ | Γ, predicted | Γ, calcd | AOM energy, X | X, predicted | X, calcd | Γ, calcd | X, calcd |
| $d_{xy}$ | $4e_\pi$ | −12.7 | −12.9 | $4e_\pi$ | −12.7 | −12.9 | −13.3 | −12.2 |
| $d_{xz}$ | $2e_\pi$ | −13.1 | −13.0 | $6e_\pi$ | −12.3 | −12.3 | −12.4 | −13.0 |
| $d_{yz}$ | $6e_\pi$ | −12.3 | −12.3 | $2e_\pi$ | −13.1 | −13.0 | −12.6 | −12.7 |
| $d_{x^2-y^2}$ | $3e_\sigma$ | −11.4 | −11.5 | $3e_\sigma$ | −11.4 | −11.5 | −10.9 | −11.8 |
| $d_{z^2}$ | $3e_\sigma$ | −11.4 | −11.3 | $3e_\sigma$ | −11.4 | −11.3 | −11.6 | −11.1 |

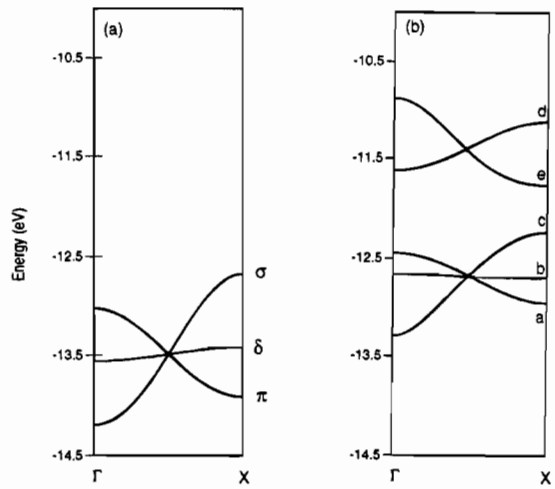


**Figure 9.** (a) Computed Ni d-orbital-based energy bands for a one-dimensional chain of Ni atoms with atomic separations appropriate to those in the cadmium halide structure. $\pi$ and $\delta$ bands are both doubly degenerate. (b) Computed energy bands for Ni d-orbital-based crystal orbitals from the one-dimensional edge-sharing chain of $NiO_6$ octahedra, including both M−O and M−M interactions.

ate here (and was used in ref 16, for example, to derive the dispersion behavior of the energy bands), since the mean positions of the bands are set by metal−oxygen interactions but their width largely by metal−metal interactions.

## Band Structures of Idealized Perovskite and Cadmium Halide Nets

We are now in a position to derive the band structure of the ideal square net derived from the cubic perovskite structure and the ideal hexagonal net of the cadmium halide structure. Results of tight-binding band structure calculations using only Ni 3d and O 2p orbitals are shown in Figure 10. The general features of the dispersion pictures of the one-dimensional chains are found here too. The $t_{2g}$ bands of both solids are now very similar in width. The perovskite net has gained additional bandwidth on moving to the two-dimensional case simply as a result of doubling the number of interactions possible for any given $t_{2g}$ orbital. No change is found for the cadmium halide structure, since the number of interactions for each $t_{2g}$ type orbital is already 4 in the one-dimensional chain. Thus, we expect little change in the bandwidths for the cadmium halide structure on moving from one to two dimensions, and indeed, this is observed. The relative dispersion of the bands of the perovskite $e_g$ set is also in keeping with the general predictions of the angular overlap model and the number of coordinated orbitals. The hexagonal net has a significantly narrower $e_g$ band than that in the perovskite net, which has again gained some additional width on moving to two dimensions. The result is a small calculated gap (on the order of 0.3 eV) between the $t_{2g}$ and $e_g$ bands for the hexagonal system. This is set by the balance of metal−oxygen interactions ($\sigma$ and $\pi$), which set the centers of the $e_g$ and $t_{2g}$ bands, and the metal−metal interactions, which contribute to their width. Certainly, though, the most dramatic feature of the perovskite band structure is the (rigorous, on symmetry grounds) absence of an energy gap between the $t_{2g}$ and $e_g$ bands, both in the two-dimensional slice through the perovskite structure and in the full three-dimensional one. This result is a simple one. The symmetry properties of the bands from Figures 4 and 10 decree that both $\sigma$ and $\pi$ bands are exactly nonbonding at the bottom of the band and thus must overlap in this way. (The computed values from Figure 10 agree well with those predicted using the results in **7**). The width of the $e_g$ band from the AOM is simply $6e_\sigma$ and the width of the $t_{2g}$ band is $8e_\pi$ in the full three-dimensional perovskite.

This result is at variance with experiment. Results from photoelectron spectroscopic studies on the perovskites $LaCoO_3$ and $LaRhO_3$ show conclusively the presence of a gap. The existence and magnitude of the $t_{2g}$−$e_g$ energy gap are crucial to understanding the electronic properties associated with these compounds.[11,13] $LaCoO_3$ (band gap 0.1 eV) exhibits an insulator to metal transition at elevated temperatures via thermal population of the upper band, while the analog $LaRhO_3$ (band gap 1.6 eV) shows no such transition but instead remains an insulator. Table 3 shows the variation in electronic properties associated with the series of $LaMO_3$ perovskites as a function of changing electron count at M. Although the crystal structures show a smooth change from a highly distorted (*Pbnm*) perovskite for $LaTiO_3$ to nearly ideal arrangements (M = Ni, Cu), the electrical properties change dramatically.[21] Their oscillating nature across the $LaMO_3$ series suggests a filling of the $t_{2g}$ band followed by a filling of the $e_g$ band. Electron correlation and exchange effects have been proposed in detail[1,22] to account for this variation in properties, but the existence of the separate $t_{2g}$ and $e_g$ bands is well established. The situation for $LaCoO_3$ is certainly more complex than presented here. We point out that a recent band structure calculation[23] on $LaCoO_3$ shows no gap between the bands. Only in cluster calculations where many-body effects are included in a dominant way is a gap found. These results suggest that the band gap in this compound is actually between the filled oxygen 2p band, which lies at an energy similar to, but slightly above, that of the filled $t_{2g}$ band, and the empty $e_g$ band. This makes the material a "charge-transfer insulator" below 937 °C. Clearly, however, the $t_{2g}$−$e_g$ separation is much smaller in $LaCoO_3$ than in $LaRhO_3$. The results described here are therefore much more applicable to the Rh case, where such effects are not as important. To understand the generation of a gap between $t_{2g}$ and $e_g$ bands, the 2p orbitals on oxygen are not sufficient, and the oxygen 2s orbitals must be added to the bonding scheme.

Wavefunctions appropriate for the symmetry points Γ and X for the one-dimensional chains corresponding to the two $NiO_2$ nets whose orbital interactions are presented in Figures 3 and 7 show quite clearly that the oxygen 2s orbitals by symmetry may mix maximally rather specifically at high-symmetry points in their respective Brillouin zones. Since the parities of the s and p orbitals are different, the symmetry points where the inter-

(21) Goodenough, J. B.; Longo, J. M. In *Landolt-Börnstein: Numerical Data and Fundamental Relationships in Science and Technology*; Hellwege, K.-H., Ed.; Springer-Verlag: New York, 1972; New Series, Vol. III/4a, p 126.
(22) Goodenough, J. B. *Magnetism and the Chemical Bond*; Wiley-Interscience: New York, 1963.
(23) Abbate, M.; Potze, R.; Sawatzky, G. A.; Fujimori, A. *Phys. Rev. B: Condens. Matter* **1994**, *49*, 7210.

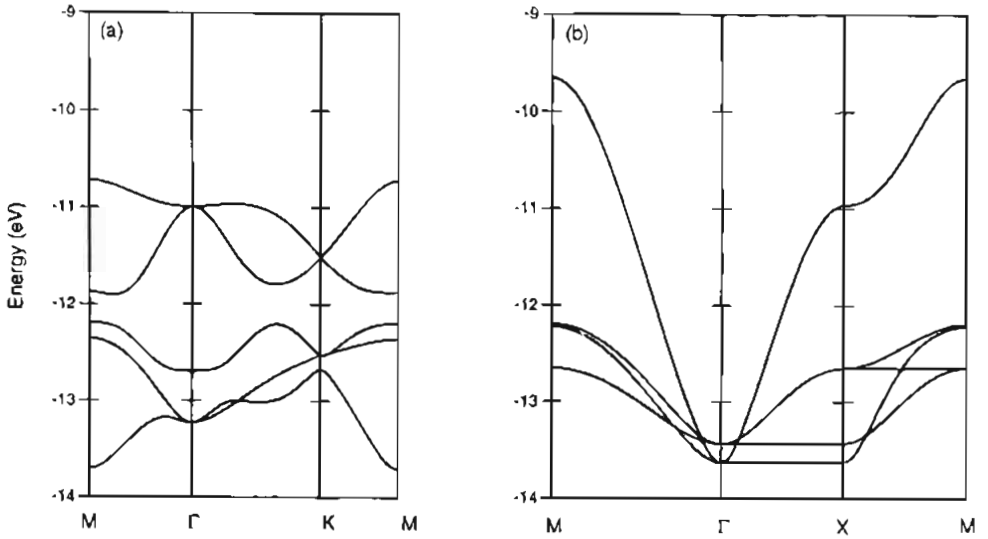


**Figure 10.** Computed band structures of the two-dimensional nets in nickel oxides employing Ni 3d and O 2p orbitals only: (a) idealized hexagonal net from $LiNiO_2$; (b) square net from $LaNiO_3$.

**Table 3.** Electronic Properties of $LaMO_3$ Perovskites

| M | electronic behavior |
|---|---|
| Ti | metal |
| V | metal−insulator transition (275 K) |
| Cr, Mn, Fe | insulator |
| Co | metal−insulator transition (664 K) |
| Ni, Cu | metal |

action between the metal and these ligand orbitals is zero will also be different. These interactions are illustrated pictorially in **10** and **11** for the perovskite and cadmium halide chains.

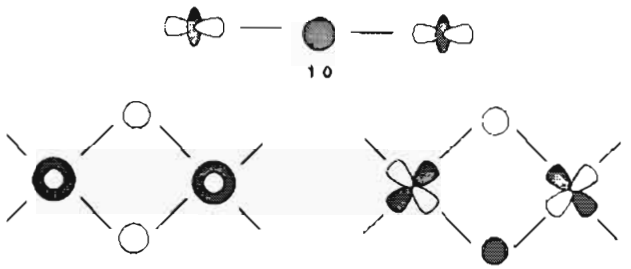

**10**



**11**

Perhaps the most important result is that, contrary to the result for the 2p orbitals, the 2s orbitals on oxygen in the net have the appropriate symmetry to mix into the perovskite $d_{z^2}$ band in an antibonding fashion at the symmetry point Γ, which has the immediate effect of raising the energy of this crystal orbital and thus shrinking the bandwidth for the perovskite. With reference to **10**, if the s orbital interaction is larger than that of the p interaction $4e_\pi$, then a band gap will open. At the X point, the zone edge, the energy of the $d_{z^2}$ band is not affected by the inclusion of the O 2s orbitals, since they cannot mix in by symmetry at this point. Thus the only effect of inclusion of O 2s orbitals into the perovskite basis is the reduction of the $e_g$ bandwidth and the possible opening of a gap in the metal d-block bands if the interaction is sufficiently large. For the cadmium halide case, the situation is again a little more complicated. At the Γ point, the $d_{z^2}$ crystal orbital should be raised in energy, while $d_{x^2-y^2}$ should remain unaffected. However, at point X, $d_{x^2-y^2}$ will be raised in energy, while $d_{z^2}$ will be unaffected. Qualitatively speaking, the $d_{x^2-y^2}$ orbital will be raised more in energy at X than $d_{z^2}$ at Γ, so the possibility exists for a switching in position of the two energy bands in the full two-dimensional band structure as a result of the inclusion of O 2s orbitals.

Figure 11 shows results of calculations carried out on the hexagonal and perovskite two-dimensional sheets, in which the effects of O 2s orbital participation have been included. As predicted, the bandwidth in the perovskite has been narrowed substantially as a result of this modification of the basis. For the hexagonal net, the effect of O 2s orbital inclusion is also rather dramatic. As seen in Figure 11a, the lower band in the $e_g$ set has been pushed up in energy to a level above that of the upper band from Figure 10a, along the symmetry line Γ−M, leading to a somewhat narrower $e_g$ band overall, although the difference is rather small. Thus inclusion of the O 2s orbitals appears to bring the electronic structures of both perovskite and cadmium halide $NiO_2$ nets more in line with what is observed experimentally. In the calculations behind Figure 11, where O 2s orbital participation has been included, the ratio of the Slater exponents for the oxygen orbitals was arbitrarily set at $\zeta(2p)/\zeta(2s) = 0.76$, indicating somewhat more participation on the part of the O 2p valence orbitals than for O 2s. (A larger value for a given Slater exponent indicates a contraction of the orbital's radial extent, thus generating a less diffuse orbital which does not overlap as well with an adjacent metal atom as does an orbital with a smaller Slater exponent.) The calculated band gap for $LaRhO_3$ is calculated to be 3.11 eV; this is to be compared with the experimental value of 1.60 eV. The correct gap may be obtained by "correct" choice of this ratio. A value of $\zeta(2p)/\zeta(2s) = 0.67$, indicating somewhat less participation on the part of O 2s than we have assumed in the above calculation, reproduces the experimental band gap.

An algebraic feel for this sensitive balance between metal d−oxygen s and p orbital interactions comes from extending the discussion of the form of the secular determinant[16] (eq 2). In the Hückel approximation this is

$$\begin{vmatrix} H_{ss} - E & 0 & 2H_{sd}\cos(ka/2) \\ 0 & H_{pp} - E & -2H_{pd}i\sin(ka/2) \\ 2H_{ds}\cos(ka/2) & 2H_{pd}i\sin(ka/2) & H_{dd} - E \end{vmatrix} = 0$$

If $H_{pp}$ and $H_{ss}$ are set equal as well as the two interaction integrals ($H_{sd} = H_{pd} = \beta$), then, using Hückel α's and β's as before, the three solutions are found to be

$$E = \alpha_p \quad (=\alpha_s)$$

$$E = \frac{(\alpha_p + \alpha_d) \pm [(\alpha_p - \alpha_d) + 16\beta^2]^{1/2}}{2} \qquad (3)$$

This result is quite dramatic. None of the energy bands have

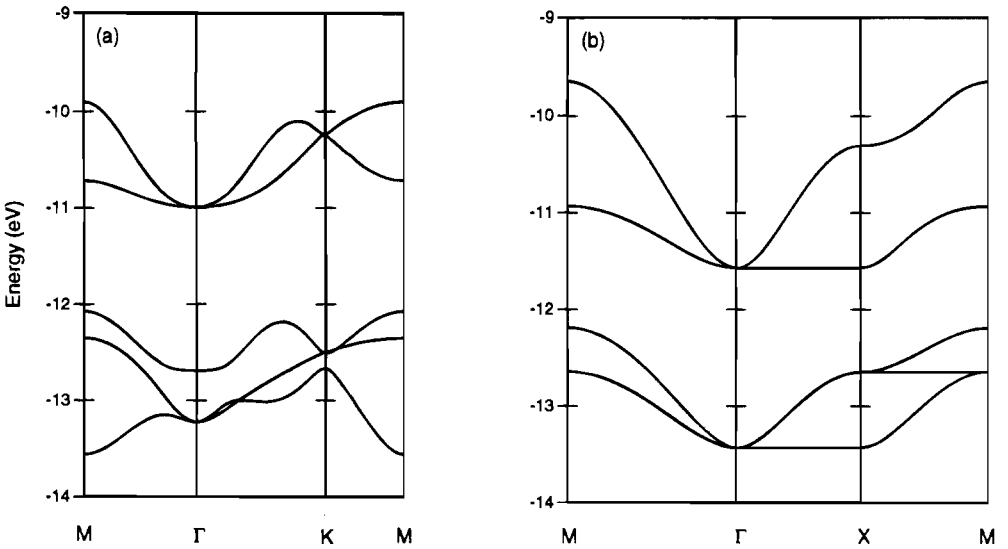


**Figure 11.** Computed band structures of the two-dimensional nets as in Figure 10, but using both O 2s and O 2p orbitals in the basis along with Ni 3d orbitals; $\zeta(2s) = 3.000$, $\zeta(2p) = 2.275$: (a) cadmium halide hexagonal net; (b) perovskite square net.

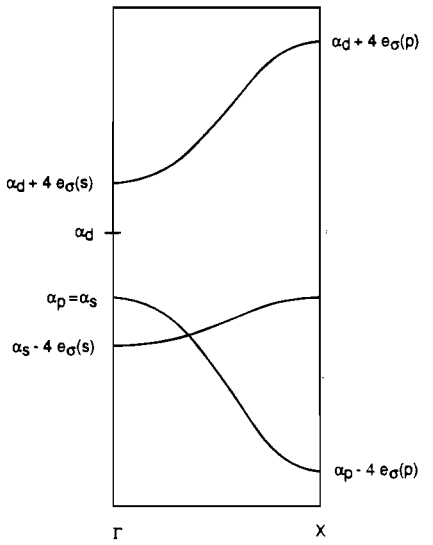


**Figure 12.** Schematic band structure sketch of the one-dimensional chain of Ni $d_{z^2}$ orbitals linked by oxygen atoms where both 2s and 2p orbitals participate in bonding interactions.

any dispersion at all; i.e., there is no $k$ dependence. If now we put $\alpha_s = \alpha_p$ but set $\beta_{sd} \neq \beta_{pd}$, the roots become

$$E = \alpha_p \quad (=\alpha_s)$$

$$E = \{(\alpha_p + \alpha_d) \pm \{(\alpha_p - \alpha_d)^2 + 16[\beta_{pd}{}^2 - \cos^2(ka/2)(\beta_{pd} - \beta_{sd})^2]\}^{1/2}\}/2 \quad (4)$$

Arbitrarily assuming that $|\beta_{pd}| > |\beta_{sd}|$, the band structure may be drawn as in Figure 12. After the usual expansion of eq 4 as a power series, these roots become

$$E = \alpha_p - \frac{4\beta_{pd}{}^2 - \cos^2(ka/2)(\beta_{pd}{}^2 - \beta_{sd}{}^2)}{|\alpha_p - \alpha_d|} \quad (5)$$

$$E = \alpha_d + \frac{4\beta_{pd}{}^2 - \cos^2(ka/2)(\beta_{pd}{}^2 - \beta_{sd}{}^2)}{|\alpha_p - \alpha_d|} \quad (6)$$

Now we are in a position to see algebraically the result easy to see above by symmetry; interaction of $d_{z^2}$ with the 2s orbital on O leads to a dispersion with a $\cos^2(ka/2)$ dependence and maximum bonding at $k = 0$, but interaction of $d_{z^2}$ with the 2p orbital on O leads to a $\sin^2(ka/2)$ dependence with maximum bonding at $k = \pi/a$. The result, if the two interactions are equal, is a dispersion-free band, and thus one of zero width. Therefore, the width of this band is determined in a vital way by the balance of the two types of interactions. Our perovskite 3d-block band structure generated by the EHTB method is in fact nearly identical to those of Mattheis[24] and Harrison[25] employing more elaborate approaches.

It is interesting to compare the factors which control the $e_g$–$t_{2g}$ gap in the extended perovskite structure with those for an isolated molecule. In the latter, $t_{2g}$ and $e_g$ orbitals are separated by $3e_\sigma - 4e_\pi$ from the AOM. Here $e_\sigma$ now represents the interaction parameter for the relevant s/p oxygen hybrid orbital which overlaps with the metal d orbitals. In the extended array, the energy difference the *middles* of the $t_{2g}$ and $e_g$ bands will be given by the same function. However, the energy difference between the top of the $t_{2g}$ and bottom of the $e_g$ bands is given as described above by a balance between $d\pi$–$p\pi$, $d\sigma$–$p\sigma$, and $d\sigma$–$s\sigma$ interactions.

Density of states (DOS) plots from the EHTB model are shown in Figure 13 for the ideal three-dimensional cubic perovskite and two-dimensional hexagonal type $NiO_2$ nets using a model including both 2s and 2p orbitals for oxygen. The Fermi level for the $d^7$ band filling occurs within the broad energy band for the perovskite type net, and so within a one-electron picture, metallic behavior is predicted for the material $LaNiO_3$. For $LiNiO_2$, the $e_g$ band is also one-fourth filled, but in contrast to the situation in perovskite, the Fermi energy lies at a high density of states, signaling the possibility of localized electrons and insulating behavior. Insight as to the origin of this high density of states may be obtained by comparing the Ni 3d/O 2p and the Ni 3d/O 2p + O 2s densities of states of Figures 10a and 11a, respectively. Notice that this rather flat part of the band responsible for this feature in the DOS is generated by the addition of the oxygen 2s orbitals. Thus the latter are of crucial importance in both systems.

## Conclusions

The thrust of this work has been an exploration of the rather dramatic symmetry-based control of the form of the band structures of two important classes of materials with the same

(24) Mattheis, L. F. *Phys. Rev. B: Solid State* **1972**, *6*, 4718.
(25) Harrison, W. A. *Electronic Structure and the Properties of Solids*; Dover: London, 1989; p 438 ff.

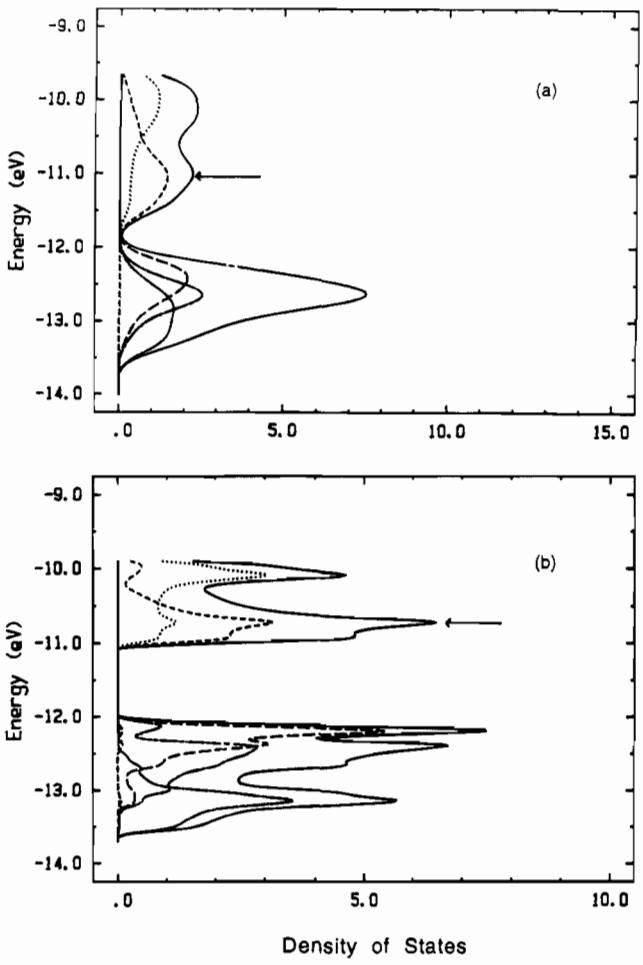


**Figure 13.** Computed density of states plots for (a) the three-dimensional cubic perovskite framework $NiO_3^{3-}$ and (b) the hexagonal two-dimensional cadmium halide net $NiO_2^-$. In both pictures, the dotted line represents the contribution from the $d_{x^2-y^2}$ orbitals on Ni, and the dashed line represents the $d_{z^2}$ contribution. The Fermi level is indicated by a horizontal arrow.

local geometry but with different extended structures. For the perovskite structure, the widths of the $t_{2g}$ and $e_g$ bands are in fact a necessary, symmetry-constrained result of the full band structure and are crucially dependent upon extended Ni—Ni interactions as well as local Ni—O interactions. The band structure of the cadmium halide net, however, can be derived in a qualitative way (as in ref 20) by adding the effects of metal—metal interaction to the levels predicted from metal—oxygen interactions only. Although the approach neglects important two-electron exchange and correlation terms in the energy, association of a narrow band having a high density of states with a localized system allows an understanding of electronic and magnetic behavior of the $LaNiO_3$- and $LiNiO_2$-type phases. A hitherto unappreciated fact is the crucial control of this electronic problem in the perovskite case by the relative importance of the interactions of oxygen 2s and 2p orbitals with the metal d orbitals. It makes it very difficult indeed to predict for the $d^6$ perovskites whether there will be a band gap or not. As we will show elsewhere,[26] this balance is also of vital importance in determining some of the properties of the high-temperature superconducting cuprates, all of which have essentially two-dimensional structures featuring the flat or nearly flat $CuO_2$ square net.[27] In this particular case, the $d_{x^2-y^2}$ band of this sheet must also be sufficiently wide (in two dimensions only) to support delocalized, metallic behavior. Its width is again controlled by this balance.

**Table 4.** Parameters Used in Extended Hückel Calculations

| atom | orbital | $H_{ii}$ (eV) | $\zeta_1$[a] | $\zeta_2$[a] | $c_1$[b] | $c_2$[b] |
|---|---|---|---|---|---|---|
| Ni | 4s | −9.17 | 1.825 | | | |
| | 4p | −5.15 | 1.125 | | | |
| | 3d | −13.49 | 5.75 | 1.64 | 0.6401 | 0.5516 |
| Co | 4s | −9.21 | 2.000 | | | |
| | 4p | −5.29 | 2.000 | | | |
| | 3d | −13.18 | 5.55 | 2.10 | 0.5680 | 0.6060 |
| Rh | 5s | −10.4 | 2.135 | | | |
| | 5p | −6.87 | 2.040 | | | |
| | 4d | −14.90 | 5.38 | 2.30 | 0.5340 | 0.6365 |
| O | 2s | −32.3 | 3.000 | | | |
| | 2p | −14.8 | 2.275 | | | |

[a] Slater-type orbital exponents. [b] Coefficients used in the double-ζ expansion.

**Acknowledgment.** This research was supported by the National Science Foundation under the auspices of the Science and Technology Center for Superconductivity (Grant DMR 9120000). We thank Dr. John F. Mitchell for many helpful discussions.

## Appendix

Calculations described in this paper were carried out using the extended Hückel method, employing the tight-binding approximation[28] for the calculation of band structures of crystalline solids. Parameters used in the calculations are collected in Table 4. Off-diagonal matrix elements have been calculated using the modified Wolfsberg—Helmholz relationship.[29] Calculations invariably involve inclusion of overlap integrals over three unit cells, except in those calculations where metal—metal interactions were excluded. In this case, the overlap integrals were evaluated out to 2.0 Å or less. (This includes the M—O interactions but excludes the M—M ones.) In density of states (DOS) calculations, a grid of 64 special K points were used in the irreducible wedge of the two-dimensional Brillouin zone appropriate for the particular square or hexagonal net. For the calculation of band structures, 51K points were chosen along each high-symmetry line enclosing the irreducible wedge of the appropriate Brillouin zone.

(26) Burdett, J. K.; Gramsch, S. A. Manuscript in preparation.
(27) A compilation of structural data on the high-temperature superconducting cuprates is to be found in: Vanderah, T. A., Ed. *Chemistry of Superconductor Materials*; Noyes: Park Ridge, NJ, 1992.
(28) Hoffmann, R. *J. Chem. Phys.* **1963**, *39*, 1397. Whangbo, M.-H.; Hoffmann, R. *J. Am. Chem. Soc.* **1978**, *100*, 6093. Whangbo, M.-H.; Hoffmann, R.; Woodward, R. B. *Proc. R. Soc. London* **1979**, *A366*, 23.
(29) Ammeter, J. H.; Bürgi, H.-B.; Thibeault, J. C.; Hoffmann, R. *J. Am. Chem. Soc.* **1978**, *100*, 3686.